P-10

A 3D Charge Model for FinFETs with Ballistic Transport

Dawei Zhang, Xue Shao, Zhiping Yu, and Lilin Tian
Institute of Microelectronics, Tsinghua University, Beijing 100084, China
Email: zdw99@mails.tsinghua.edu.cn

Abstract - An analytical charge model is proposed for 3D FinFETs. The model is based on a self-consistent solution to 2D Poisson's and Schrödinger equations with closed form. In conjunction with the ballistic transport along the channel, the device *I-V* characteristics is predicted. Through comparison with results from numerical and experimental data, the correctness of the model has been established.

I. INTRODUCTION

The superior performance of double-gate FETs (DG-FETs) and FinFETs warrants the multi-gate structure a strong contender beyond planar bulk CMOS devices [1-2]. For IC designers, compact models for this type of devices are urgently needed. There has been excellent work on charge modeling for general [3] and UTB (ultra-thin body) [4] DG-FETs. The major challenge in these models is to find a closed-form solution to the coupled Poisson's and Schrödinger equations. This task is relatively easy to tackle in 1D (the channel cross-section in DG-FETs is such a case) but rather difficult in 2D, where FinFET structures fall. This is the reason why relatively few work has been done in this aspect [5].

We present in this paper a comprehensive approach to the self-consistent solution of 2D Poisson's and Schrödinger equations. A closed-form for line-charge density has been developed as the function of the applied gate bias. Analytical model for threshold voltage then follows naturally. The *I-V* characteristics for FinFET devices are obtained through incorporating the ballistic transport along the channel.

II. 2D ANALYTICAL SOLUTION TO POISSON AND SCHRODINGER EQUATIONS

The cross-section of a FinFET is illustrated in Fig. 1. The silicon channel is surrounded by oxide with three different thicknesses: t_{ox1} for two side gates, t_{ox2} for top gate, and t_{ox3} for the buried oxide. The width (b) direction is taken as x-axis, and height (a) y-axis. The main objective is to obtain an analytical expression linking the channel integral charge Q_{inv} (per unit channel length, or called line density) with the applied gate bias V_G (and the channel voltage) by solving Poisson's and Schrödinger equations self-consistently on the 2D cross-section of the channel (or fin).

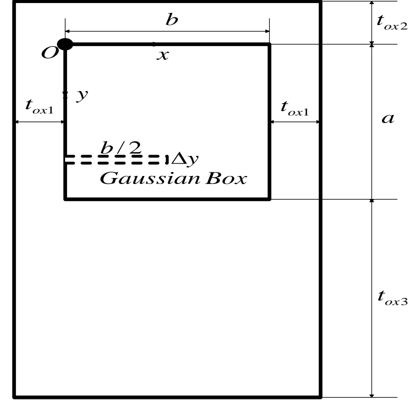

Fig.1: Schematic of the cross-section for a FinFET.

The procedure to obtain the analytical solutions to these two equations is outlined as follows:

1. Similar to the approach used in [3], 2D trial wavefunctions $\psi_{i,j}(x,y)$ are proposed for Schrödinger equation at the cross-section of the channel with two parameters ($b_{x,i}$ and $b_{y,j}$) to be determined (see below). The wavefunctions are used to represent the density of states or probability of carrier distribution in real space ($a_{x,i}, a_{y,j}$ are normalization factors and i, j are quantum numbers):

$$\psi_{i,j}(x,y) = \left(a_{y,j}/\sqrt{2/a}\right)\sin\left[(j+1)\pi y/a\right]e^{-b_{y,j}y/a}$$
$$\times\left(a_{x,i}/\sqrt{2b}\right)\sin\left[(i+1)\pi x/b\right]\left(e^{-b_{x,i}x/b}+e^{-b_{x,i}(b-x)/b}\right) \quad (1)$$

2. The multiplication of Q_{inv} and $\psi_{0,0}$ is substituted into the right side of the Poisson's equation to represent the charge distribution. The original Poisson's equation is then decomposed into two problems: Poisson's equation with homogeneous boundary conditions and Laplace equation with the specified boundary conditions. The former is solved by using Green's function and the latter solved by the separation-of-variables. The silicon region is bloated from $[0,b]$ to $[-x_1, b+x_1]$ and $[0,a]$ to $[-y_1, a+y_2]$ ($x_1 = t_{ox1}\varepsilon_{si}/\varepsilon_{ox}$, $y_1 = t_{ox2}\varepsilon_{si}/\varepsilon_{ox}$ and $y_2 = t_{ox3}\varepsilon_{si}/\varepsilon_{ox}$) to "eliminate" the Si/SiO2 interface (following the approach in [5]). The derived electric potential $\Phi(x,y)$ is shown:

$$\Phi(x,y) = \underbrace{\sum_{m=1}^{\infty}\sum_{n=1}^{\infty}A_{mn}\Psi_{mn}(x,y)}_{\text{particular solution from Poisson's equation}} +$$

$$\underbrace{V_G - \Phi_{MS} + \left[-\left(V_G - V_B\right)y/y_2 + a\left(V_G - V_B\right)/y_2\right]u\left(y-a\right)}_{\text{general solution from Laplace equation}} \quad (2)$$

with Φ_{MS} the work function difference between gate region and silicon channel region, V_B the substrate contact bias and $u(x)$ the step function. A_{mn} is a function of structural parameters, $b_{x,i}$, $b_{y,j}$ and Q_{inv} while $\Psi_{mn}(x,y)$ is the eigen-function of Green's function method. To show this model's applicability, we compared the analytical potential with numerical ones in Fig. 2 with a device of $t_{ox3} = 3\text{nm}$ $a = 4\text{nm}$, $b = 3\text{nm}$, $t_{ox1} = t_{ox2} = 1\text{nm}$ at $V_G = 0.6\text{V}$. The results demonstrate the accuracy of our model.

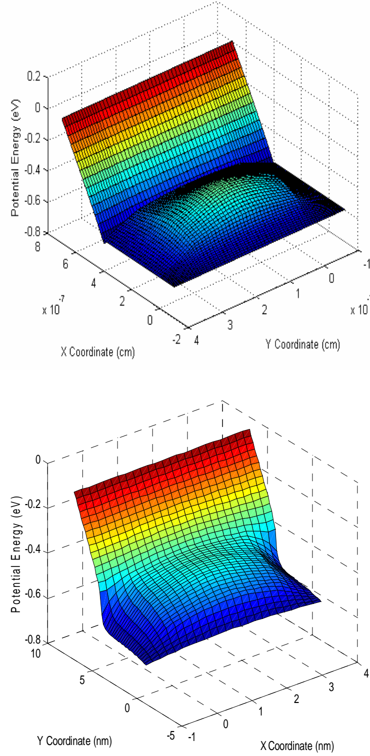

Fig. 2: Comparison of the electric potential energy between numerical (lower figure) and analytical (upper figure) results. $a = 4\text{nm}$, $b = 3\text{nm}$, $t_{ox1} = t_{ox2} = 1\text{nm}$, $t_{ox3} = 3\text{nm}$, $N_A = 1e10$ cm^{-3} and $V_G = 0.6\text{V}$.

3. 2D Schrödinger equation is then solved by substituting both trial wavefunctions and electric potential. The eigen-energies are derived by multiplying both sides with the complex conjugate eigen-function and integrating over the entire cross-section. The results are:

$$\left\langle E_{i,j}\right\rangle = \underbrace{\frac{(i+1)^2\hbar^2\pi^2}{2m_x b^2}\left[1 - \frac{b_{x,i}^2}{(i+1)^2\pi^2} + \frac{b_{x,i}a_{x,i}^2\left(1-e^{-2b_{x,i}}\right)}{2\left[b_{x,i}^2 + (i+1)^2\pi^2\right]}\right]}_{\text{kinetic energy in width direction}}$$

$$+ \underbrace{\frac{(j+1)^2\hbar^2\pi^2 a_{y,j}^2\left(1-e^{-2b_{y,j}}\right)}{4m_y a^2 b_{y,j}}}_{\text{kinetic energy in height direction}}$$

$$- \underbrace{2q\sum_{m=1}^{\infty}\sum_{n=1}^{\infty} A_{mn}C_m^i D_n^j / \sqrt{(a+2x_1)(b+y_1+y_2)}}_{\text{potential energy resulted from particular solution}}$$

$$\underbrace{-q\left[V_G - \Phi_{MS}\right]}_{\text{potential energy resulted from general solution}} \quad (3)$$

The variational approach is then used to obtain transcendent equations for $b_{x,i}$, $b_{y,j}$. For the sake of computational efficiency, explicit expressions are used [3] for $b_{x,i}$, $b_{y,j}$, i.e.,

$$b_{x,i} = b\left\{q^2 m_x\left(N_A b + cof_1\frac{Q_{inv}}{qa}\right)/\left[4(i+1)\varepsilon_{si}\hbar^2\right]\right\}^{1/3}$$

$$b_{y,j} = a\left\{q^2 m_x\left(N_A a + cof_2\frac{Q_{inv}}{qb}\right)/\left[4(j+1)\varepsilon_{si}\hbar^2\right]\right\}^{1/3} \quad (4)$$

Where cof_1 and cof_2 are fitting parameters later used in the compact model with default values 5/6. In Fig. 3, the comparisons of eigen-energy levels are made between the self-consistent analytical solution and numerical simulations. The results demonstrate satisfactory accuracy.

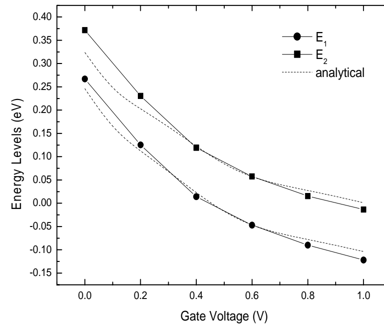

Fig. 3: Comparison of the energy levels. Symbols with solid lines are numerical results. The device structure and bias condition are: $a = 3\text{nm}$, $b = 4\text{nm}$, $t_{ox1} = t_{ox2} = 1\text{nm}$, $t_{ox3} = 3\text{nm}$, $N_A = 1e10\text{cm}^{-3}$ and $V_G = 0.6\text{V}$.

III. IMPLICIT CHARGE MODEL AND DEFINITION OF LINE-EFFECTIVE-DENSITY-OF-STATES (LEDOS)

For FinFETs, different from DG-MOSFETs, the carriers in the channel region act as 1D quantum gas, meaning that the carrier moves freely only in the transport direction with both of the other two directions strongly confined. In this case, the line density of the mobile charge is

derived as:

$$Q_{inv} = \sum_{i=1}^{N_x}\sum_{j=1}^{N_y}\sum_{k=1}^{N_v} 2q\hbar\sqrt{2m_{z,k}^{*}k_BT/\pi}$$
$$\times\exp\left[-\left(E_{i,j,k}-E_{Fn}\right)/k_BT\right] \quad (5)$$

With k referring to different valleys of the silicon conduction band, $m_{z,k}^{*}$ the effective mass along the transport direction of valley k, $E_{i,j,k}$ energy levels and E_{Fn} the electron Fermi level in the channel. Eq. (5) provides us with an implicit form of Q_{inv}. However, due to the non-linearity of $E_{i,j,k}$ to Q_{inv}, in strong inversion region, Eq. (5) cannot be directly used to obtain Q_{inv}. We define an LEDOS, N_{LEDOS}, as the integral of the 1D density of states in the energy space after the modulation according to the probabilities of the carriers' occupations of respective energy levels, i.e.,

$$N_{LEDOS}\left(Q_{inv}\right) = \sum_{i=1}^{N_x}\sum_{j=1}^{N_y}\sum_{k=1}^{N_v} 2\hbar\sqrt{2m_{z,k}^{*}k_BT/\pi}$$
$$\exp\left[-\left(E_{i,j,k}-E_C\right)/k_BT\right] \quad (6)$$

Where $E_C = -q\phi_C$ with ϕ_C the minimum point of the electric potential at the cross-section. Eq. (5) then can be compactly rewritten as $Q_{inv} = qN_{LEDOS}\exp\left(q\phi_C/k_BT\right)$ where the Fermi level is taken as the potential reference. The advantage of introducing N_{LEDOS} is that it trades the nonlinear relationship between $E_{i,j,k}$ and Q_{inv} to E_C and Q_{inv} so that during the iterations for Q_{inv}, N_{LEDOS} stays roughly constant. Then Q_{inv} and ϕ_C have a simple exponential relationship. On the other hand, according to Eq. (2), another relation of Q_{inv} to ϕ_C will be obtained, i.e. $Q_{inv} = C_G\left[V_G - \Phi_{MS} - \phi_C - S\left(N_A\right)\right]$ with $C_G = -\lambda_{mn}\varepsilon_{si}a_{eff}b_{eff}/\sum_{m=1}^{\infty}\sum_{n=1}^{\infty}4C_m^0D_n^0\Psi_{mn}\left(b/2, y_{\min}\right)$ and $S\left(N_A\right)$ a function of structural parameters and channel doping N_A. With these two independent relations between Q_{inv} and ϕ_C, the iteration strategy is developed to obtain Q_{inv}. In Fig. 4, the carrier densities (Q_{inv}/q) from the iteration are compared to the numerical simulation using the same device structure as in Fig. 2. It is seen that the model has good agreement with the simulation results.

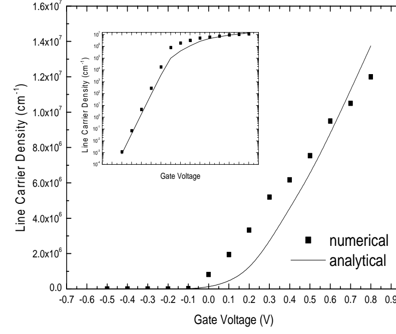

Fig. 4 Comparison of the line carrier density between numerical (dots) and analytical (lines) results. The logarithmic scale is also shown on the top-left. The device structure: $a = 4$nm, $b = 3\text{nm}, t_{ox1} = t_{ox2} = 1\text{nm}, t_{ox3} = 3\text{nm}, N_A = 1e10\text{cm}^{-3}$.

IV. COMPACT CHARGE AND *I-V* MODEL

Using the similar form for the universal compact charge model for MOSFETs [6], the compact model for FinFETs is proposed as follows:

$$Q_{inv} = C_{G0}2\phi_t\ln\left(1+\exp\left(\left(V_G-\Phi_{MS}-S\left(N_A\right)-\phi_C\right)/2\phi_t\right)\right)/$$
$$\left[1+\frac{2\phi_tC_{G0}}{qN_{LEDOS0}}\times e^{\frac{\left(V_G-\Phi_{MS}-S\left(N_A\right)-\phi_C-2\left(V_G-\Phi_{MS}-S\left(N_A\right)-V_{off}\right)\right)}{2\phi_t}}\right] \quad (7)$$

Furthermore, with the application of the ballistic transport [7], a compact *I-V* model has been developed considering all the subbands and valleys of the 1D electron gas. This model has only five fitting parameters and is therefore easy for parameter extraction. In Fig. 5, the carrier density calculated by the compact model is compared with the numerical results.

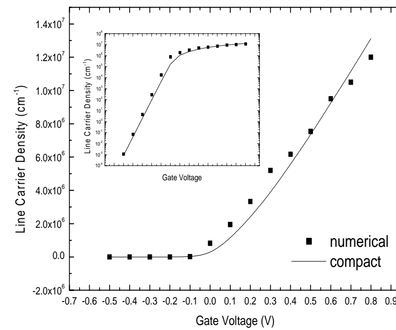

Fig. 5 Comparison of the line carrier density between numerical (dots) and compact (lines) results. The logarithmic scale is also shown on the top-left. The device structure: $a = 4$nm, $b = 3\text{nm}, t_{ox1} = t_{ox2} = 1\text{nm}, t_{ox3} = 3\text{nm}, N_A = 1e10\text{cm}^{-3}$.

It is evident that the compact model is in

better accordance with the numerical simulation than the implicit form due to the parameter fitting. In Fig. 6, the transfer characteristics calculated by our model for a 10nm FinFET [2] are depicted, showing satisfactory consistency with the measured data [2].

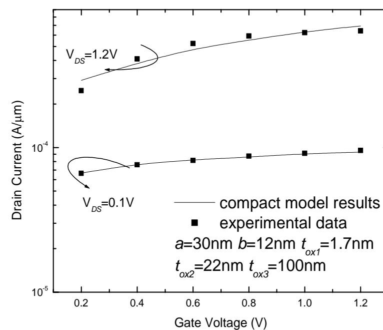

Fig. 6 Drain current versus gate voltage under different drain bias. The device structure is from [2].

V. CONCLUSIONS

The universal compact charge model for FinFETs has been developed based upon a self-consistent, analytical solution to 2D Schrödinger and Poisson's equations. Utilizing ballistic transport, a complete *I-V* model is then established. Through comparison to numerical and experimental data, this compact model correctly predicts the charge density and the DC current of FinFETs.

REFERENCES

[1]Y. Choi, *et al.*, IEDM *Tech Digest*, p. 421, Dec. 2001.

[2] B. Yu, *et al.*, *IEDM Tech Digest*, p. 251, Dec. 2002.

[3] L. Ge, *et al.*, *Trans. Electron Devices*, Vol. 49, p. 287, 2002.

[4] G. Baccarani, *et al.*, *Electron Devices,*Vol. 46, p.1656, 1999.

[5] G. Pei, *et al.*, *Trans. Electron Devices*, Vol. 49, p. 1411, 2002.

[6] Y. Ma, *et al.*, *Trans. CADICS*, Vol.20,p.495, 2001.

[7] D. Zhang et al., *Nanotech 2004*, Vol. 2, p. 56, 2004.